

Biphonons in the Klein-Gordon lattice

Laurent Proville

Service de Recherches de Métallurgie Physique, CEA/DEN/DMN Saclay 91191-Gif-sur-Yvette Cedex, France

(Dated: May 3, 2019)

A numerical approach is proposed to compute the phonon bound states in a quantum nonlinear Klein-Gordon lattice. In agreement with other studies^{1,2} on a different quantum lattice, nonlinearity is found to lead to a phonon pairing and consequently some biphonon excitations. The energy branch and the correlation properties of the Klein-Gordon biphonon are studied in detail.

PACS numbers: 63.20.Ry, 03.65.Ge, 11.10.Lm, 63.20.Dj

I. INTRODUCTION

In lattices made of identical particles, the energy is formulated by the Hamiltonian operator:

$$H = \sum_l \left[\frac{p_l^2}{2m} + V(x_l) + \sum_{j=\langle l \rangle} W(x_l - x_j) \right]. \quad (1)$$

where x_l and p_l are displacement and momentum of the particle at site l , in a d -dimensional lattice. From the left to the right hand side of the equation Eq.1, the energy contributions are identified as the kinetic energy, the local potential and the interaction between particles. Our purpose is to study the case of quantum particles that are weakly interacting, i.e., the onsite energy V dominates the interaction W . Physically, this can account for the coupling of internal modes in molecular crystals. For small amplitudes of x_l , the well-known harmonic approximation reduces H to a sum of quadratic terms, i.e., the linear Klein-Gordon (KG) Hamiltonian. So, the Schrödinger equation can be solved analytically. The elementary excitation is a plane wave called an *optical phonon* and whose energy is fixed by the wave momentum q , in the lattice Brillouin zone. A consequence of the ideal harmonicity is that higher order excitations are simply the linear superpositions of these optical phonons.

For larger displacements, some non-quadratic contributions are involved in the expansion of H . Then the nonlinear KG Hamiltonian can no longer be diagonalized analytically. In a nonlinear KG lattice, F. Bogani³ derived some one- and two- phonon renormalized Green functions and showed that the nonlinear terms involve a pairing of the optical phonon modes. It confirmed the existence of biphonon excitations, studied earlier in a different lattice model by V.M. Agranovich⁴. A convincing agreement was found between theory³ and experiments^{5,6} in molecular crystals where the internal molecule bonds yield a strong nonlinearity. The direct diagonalization of a KG Hamiltonian is, in principle, more precise than the computation of Green functions since it requires fewer approximations. In Ref. 7, by treating numerically the KG model, W. Z. Wang *and al.* confirmed the existence of phonon bound states. Furthermore, some of these states have been shown to feature a particle-like energy band, for certain model parameters. The authors identified these specific excitations as being some quantum breathers (see Refs. 2,8,9,10,11 for more details about quantum breathers) because of their counterparts in classical mechanics^{12,13}. Nonetheless, the approach proposed in Ref. 7 requires a huge computing cost so the size of lattices was limited to a one-dimensional (1D) chain of 8 unit cells. Moreover, the numerical simulations were restricted to the parameter region where the non-harmonic part of the lattice energy is modelled by a quartic onsite potential, i.e., the well-known ϕ^4 model. In the present paper, we propose a numerical treatment of the nonlinear KG lattice which takes advantage of the weak coupling (W in Eq.1). That permits to analyze lattices large enough to approach the infinite system features and to study different types of nonlinearity, as well as the two-dimensional (2D) KG lattice.

We confirm that when nonlinearity is significant, a pairing of optical phonon states occurs and the so-called biphonon¹ branch contributes to the energy-spectrum. That branch splits from the two-phonon band by opening a gap. The width of that gap indicates the magnitude of nonlinearity since the biphonon gap vanishes completely for a pure harmonic lattice. In between the two types of lattice, i.e., harmonic and strongly nonlinear, the binding energy of the biphonon drops to zero at the center of the lattice Brillouin zone (BZ) while at the edge, the biphonon excitations are still bound. Then, in the energy-spectrum, the biphonon gap vanishes at the center, whereas a pseudogap is found to open at the edge of BZ. We predict that the pseudogap is a systematic feature of lattices in which nonlinearity is moderate, whatever is the lattice dimension or the dominant nonlinearity, i.e., ϕ^3 or ϕ^4 . In addition, we enhance how quantum properties of the biphonon depends on the nonlinearity. When the biphonon gap opens, the Klein-Gordon biphonon excitations show a finite correlation length, for all momentum q , under the condition that the non-quadratic energy term is a ϕ^4 potential. That agrees with findings of Ref.7. Considering the cubic term in the potential energy V , it involves a long range correlation of the biphonon states. The space correlation properties

of triphonon are also studied and our results are used to establish some expectations on the existence of breather-like excitations in the quantum KG lattice.

The present paper is organized as follows. In Sec.II the model for the nonlinear discrete lattice is introduced and the computing method is detailed. Then it is tested for the quadratic lattices as well as for the ϕ^4 model. In Sec.III our results are presented concerning the biphonon spectrum while in Sec.IV the space correlation properties of the phonon bound states are studied. Finally, these results are discussed in Sec.V.

II. MODEL AND COMPUTING METHOD

In Eq.1, at node l of a translational invariant d -dimensional lattice, the quantum particle of mass m evolves in a local potential V , being coupled to its nearest neighbours, j by the interaction W . For moderate amplitudes of mass displacements around equilibrium, V and W can be expanded as Taylor series. The expansion of V is truncated to the fourth order $V(x_l) = a_2 x_l^2 + a_3 x_l^3 + a_4 x_l^4$ while for W , only the quadratic term is retained, $W(x_l - x_j) = -c(x_l - x_j)^2$. Higher order terms can be treated with no difficulty in what follows. Actually, they are found not to change qualitatively the results, at least for reasonable values of energy coefficients, consistent with optical modes.

Introducing the dimensionless operators $P_l = p_l/\sqrt{m\hbar\Omega}$, $X_l = x_l\sqrt{m\Omega/\hbar}$ where the frequency $\Omega = \sqrt{2(a_2 - 2.c.d)/m}$ is defined for either a chain $d = 1$ or a square lattice $d = 2$, the Hamiltonian reads

$$H = \hbar\Omega \sum_l \frac{P_l^2}{2} + \frac{X_l^2}{2} + A_3 X_l^3 + A_4 X_l^4 + \frac{C}{2} X_l \sum_{j=\langle l \rangle} X_j \quad (2)$$

where one finds the dimensionless coefficients:

$$A_3 = a_3 \sqrt{\frac{\hbar}{m^3 \Omega^5}}, \quad A_4 = a_4 \frac{\hbar}{m^2 \Omega^3} \quad \text{and} \quad C = \frac{4c}{m\Omega^2}.$$

For the harmonic lattice, i.e., $A_3 = 0$ and $A_4 = 0$, the Fourier transform of both the displacements, $X_l = \frac{1}{\sqrt{S}} \sum_q e^{-iq \times l} \tilde{X}_q$ and the momenta, $P_l = \frac{1}{\sqrt{S}} \sum_q e^{-iq \times l} \tilde{P}_q$ simplifies H into a sum of independent Hamiltonian:

$$h_q = \hbar\Omega \left(\frac{\tilde{P}_q^2}{2} + \frac{\omega_q^2}{2} \tilde{X}_q^2 \right) \quad (3)$$

with $\omega_q = \sqrt{1 - 2C \sum_k \cos(q_k)}$ and q_k is the dimensionless coordinate of the wave vector in the k^{th} direction of the lattice. The periodic boundary conditions impose $q_k = 2\pi l_k/L_k$ where L_k is the number of sites in the k^{th} direction and l_k is an integer $l_k \in [1, L_k]$. The lattice size is denoted $S = \prod_{k=1}^d L_k$. Using the standard harmonic oscillator theory, one finds the eigenvalues:

$$\Lambda_{\{n_q\}} = \hbar\Omega \sum_q \left(n_q + \frac{1}{2} \right) \sqrt{1 + 2C \sum_k \cos(q_k)}. \quad (4)$$

The n_q are quantum numbers that range from 0 to infinity and fix the energy contribution of the mode q . For the nonlinear case, the aforementioned procedure is no longer simple because non-quadratic terms yield a coupling between the h_q operators. Indeed, writing the nonlinear energy term ($\sum_l X_l^3$) as a function of the displacements Fourier transform \tilde{X}_q , gives $(\frac{1}{\sqrt{S}} \sum_{q,q'} \tilde{X}_q \tilde{X}_{q'} \tilde{X}_{(-q-q')})$. The computation of the corresponding bracket thus scales as S^2 as the sum runs over 2 wave vector, while for the quartic term it would scale as S^3 . Such a task has been achieved in Ref.7 for the quartic term. In the algorithm which follows, the computation of the brackets in Eq.8, scales as S which requires much less computation time for a given S . Starting from the exact diagonalization of the Hamiltonian where no interaction couples displacements, the low energy states are used to construct a set of Bloch waves upon which is expanded the entire Hamiltonian, including the coupling W . The Schrödinger equation is then approximately solved with an error which shrinks to zero by increasing the basis cutoff.

The starting point is thus the eigenvalue problem for a single oscillator $h_l = \hbar\Omega(\frac{P_l^2}{2} + \frac{X_l^2}{2} + A_3 X_l^3 + A_4 X_l^4)$. The Bose-Einstein operators $a_l^+ = (X_l - iP_l)/\sqrt{2}$ and $a_l = (X_l + iP_l)/\sqrt{2}$ are introduced in the writing of h_l :

$$h_l = \hbar\Omega \left[a_l^+ a_l + \frac{1}{2} + \frac{A_3}{\sqrt{8}} (a_l^{+3} + a_l^3 + 3a_l^+ a_l^2 + 3a_l^{+2} a_l + 3a_l^+ + 3a_l) \right. \\ \left. + \frac{A_4}{4} (a_l^{+4} + a_l^4 + 4a_l^{+3} a_l + 4a_l^+ a_l^3 + 6(a_l^{+2} a_l^2 + a_l^{+2} + a_l^2 + 2a_l^+ a_l) + 3) \right]. \quad (5)$$

Expanding the operator h_l on the Einstein states, i.e., $|n, l\rangle = \frac{1}{\sqrt{n!}} a_l^{\dagger n} |\emptyset_l\rangle$ for all $n \in \{0 \dots N-1\}$ gives a matrix \mathcal{M} of rank N . In each row of \mathcal{M} , one finds the nonzero coefficients:

$$\begin{aligned}\mathcal{M}_{n,n} &= \frac{3}{2}A_4n^2 + n(3A_4 + 1) + \frac{3}{4}A_4 + \frac{1}{2} \\ \mathcal{M}_{n,n+4} &= \frac{1}{4}A_4\sqrt{(n+4)(n+3)(n+2)(n+1)} \\ \mathcal{M}_{n,n+3} &= \frac{1}{\sqrt{8}}A_3\sqrt{(n+3)(n+2)(n+1)} \\ \mathcal{M}_{n,n+1} &= \frac{3}{\sqrt{8}}A_3\sqrt{(n+1)^3} \\ \mathcal{M}_{n,n+2} &= \frac{1}{4}A_4(4n+6)\sqrt{(n+2)(n+1)}.\end{aligned}\quad (6)$$

When the cutoff N tends to infinity, the Einstein states form a basis in the space of onsite states. The Schrödinger problem for the Hamiltonian h_l is thus equivalent to the diagonalization of \mathcal{M} . That diagonalization is compared to the semi-classical quantization¹⁴ in Fig. 1(a), for the case of a He atom embedded into a double-well potential: $V(x) = 16E_d/b^4x^2(x-b)^2$. The parameters, E_d and b , are the energy barrier and distance between minima, respectively (see Ref. 15). The very good agreement proves the efficiency of the diagonalization method even for a non-monotonic onsite potential. Arranging the onsite eigenstates in increasing order of their eigenvalues, the α^{th} eigenstate is denoted $\phi_{\alpha,i}$ and its eigenvalue is $\gamma(\alpha)$. As shown in Fig.1(b), each eigenvalue $\gamma(\alpha)$ is found to converge to a steady value as N increases. In Fig.1 (b), the graphic does not allow to distinguish $N = \infty$ from $N > 100$. With today's computers, the cutoff has been easily increased to $N = 2000$ which has been taken for the limit $N = \infty$ in Fig.1(b). Increasing the cutoff to values larger than $N = 100$ does not change significantly our final results on the low energy excitations of the KG lattice (Sec.III). In what follows, N is cautiously fixed to $N = 500$ and then the time requirement to diagonalize \mathcal{M} is about few minutes on a PC computer. Note that increasing N implies no overload of the calculations in the second part of the algorithm.

We now treat lattices with non-zero inter-site coupling. The onsite state products $\Pi_i \phi_{\alpha_i,i}$ form a complete orthogonal base for the lattice states. In order to reduce the computer memory requirement, one takes advantage of the translation invariance by introducing the Bloch wave formulation for the state products. Among those states some equivalence classes can be constructed in which each state results from a translation applied to another state of the same class. Retaining only one element for each translation class, the state which represents the class is identified by the series of its α_i 's, that is denoted $[\Pi_i \alpha_i]$. The construction of the equivalence classes is performed numerically. For each class, a Bloch wave can be written as follows:

$$B_{[\Pi_i \alpha_i]}(q) = \frac{1}{\sqrt{A_{[\Pi_i \alpha_i]}}} \sum_j e^{-iq \cdot j} \Pi_i \phi_{\alpha_i, i+j} \quad (7)$$

where $A_{[\Pi_i \alpha_i]}$ ensures the normalization. Some attention must be paid to the possible translation symmetry of the state products that may be higher than the lattice symmetry. Indeed, for a given product there may be a lattice vector t that verifies $\Pi_i \phi_{\alpha_i, i} = \Pi_i \phi_{\alpha_i, i-t}$ with coordinates t_k such as $t_k < L_k$. It implies that $A_{[\Pi_i \alpha_i]} = S \prod_{k=1}^d (L_k/t_k - fc(L_k/t_k))$ where $fc(L_k/t_k)$ is the fractional portion of the ratio L_k/t_k . Then the Bloch wave can only take the momentum q such as $q_k = 2\pi p_k/L_k = 2\pi p'_k/t_k$ where p_k and p'_k are some different integers. The set of states $\{B_{[\Pi_i \alpha_i]}(q)\}_{q, N_{cut}}$, including the uniform state $\Pi_i \phi_{0,i}$ at $q = 0$, form a truncated basis where N_{cut} fixes the upper boundary on the onsite excitations: $\sum_i \alpha_i \leq N_{cut}$. When C is negligible, these states are the eigenstates of H . For moderate values of C , they should be good approximates. Since the Bloch waves with different q , are not hybridized by H , the Hamiltonian can be expanded separately for each q . It is performed analytically and gives a matrix $\mathcal{B}(q)$ the coefficients of which are written as follows:

$$\begin{aligned}\langle B_{[\Pi_i \alpha_i]}(q) | H | B_{[\Pi_i \beta_i]}(q) \rangle = & \frac{1}{\sqrt{A_{[\Pi_i \alpha_i]} A_{[\Pi_i \beta_i]}}} [\Pi_i \delta_{\alpha_i, \beta_i} \sum_i \gamma(\alpha_i) - \frac{C}{2} \sum_{l,j} \exp(-iq \times j) \\ & \sum_{k=\langle l \rangle} D(\alpha_l, \beta_{l+j}) D(\alpha_{l+k}, \beta_{l+k+j}) \Pi_{i \neq l, l+k} \delta_{\alpha_i, \beta_{i+j}}] \end{aligned} \quad (8)$$

where $D(\alpha_l, \beta_l)$ denotes the bracket $\langle \phi_{\alpha_l} | X_l | \phi_{\beta_l} \rangle$ that is given by:

$$D(\alpha_i, \beta_i) = \frac{1}{\sqrt{2}} \sum_{l=0}^N \langle \phi_{\alpha_i, i} | l, i \rangle (\sqrt{l+1} \langle l+1, i | \phi_{\beta_i, i} \rangle + \sqrt{l} \langle l-1, i | \phi_{\beta_i, i} \rangle). \quad (9)$$

The eigenvalues of $\mathcal{B}(q)$ are computed numerically with an exact Householder method¹⁶. In Fig. 2, for a 1D chain $S = 4$, our calculation is compared to Ref. 7 (see Ref. 17 for conversion of model parameters). A very good agreement is noted for the low energy states since the eigen-spectra are superposed in Fig. 2. In Ref. 7, the Schrödinger equation was solved by diagonalization of the matrix obtained from expanding H in the Einstein phonon basis, i.e., the eigenstates of the pure harmonic lattice (see Eq.3). According to the authors : “it restricts the numerical simulations to a parameter region where nonlinearity is not too large”. In contrast, thanks to the first step of our algorithm which solves the single site nonlinear eigenvalue problem, we can treat all types of nonlinearity (weak or strong and with ϕ^3 or ϕ^4 terms), provided the inter-site coupling is not too large. For instance, the approach of Ref.7 requires some computations even for $C = 0$ if $A_3 \neq 0$ or $A_4 \neq 0$, which is straightforwardly solved in the first step of the present algorithm. Within the second step, in order to estimate the accuracy of our calculations, different lattice sizes have been tested for a reasonable value of C ($C = 0.05/d$, see Sec. III) and different A_3 and A_4 . For small sizes, N_{cut} can be stepped up sufficiently to make eigenenergies converge to steady values. The convergence is as fast as C is small, i.e., when $C = 0$ the computation is exact (to machine precision) and near instantaneous whereas when C is raised, the accuracy becomes worse because of inter-site coupling terms: $(a_i^+ a_j^+)$ and $(a_i a_j)$ that involve hybridization with high energy Bloch waves (Eq.7), above the cutoff. Once N_{cut} has been determined to achieve the required precision, then the lattice size is increased up to the capacity of our computer memory. For instance, in a 1D lattice with $S = 17$, N_{cut} has been varied from $N_{cut} = 3$ (68 Bloch waves, Eq.7) to $N_{cut} = 6$ (5940 Bloch waves). For $N_{cut} = 4$, the error on the low energy eigenvalues, say the 2 phonon states, is inferior to 1% in comparison with $N_{cut} = 6$. The size has thus been increased to $S = 33$ (3052 Bloch waves) with no noticeable discrepancy of the eigen-spectrum. For such a lattice, the time required for the computation of the matrix $\mathcal{B}(q)$ scales in minutes whereas the diagonalization requires few hours with a PC. This can be reduced to some minutes with a vectorial computer and suitable numerical libraries. The matrices we have to treat are much smaller than those in Ref.7, which accounts for the tractability of our method. For $S = 4$, 65536 states were required in Ref.7 whereas only 19 Bloch waves were required in our calculations for the same lattice, with same parameters (see Fig.2). This increase in efficiency has been possible because we took advantage of the weak inter-site coupling. For the 2D lattices, the size has been limited to $S = 13 \times 13$ which involves 4931 Bloch waves with $N_{cut} = 3$. Some improvements are under investigation. For example, the number of required states can be reduced again by imposing $\alpha_i < n_{low}$ for Bloch waves that verify $\sum_i \alpha_i > N_{low}$ in Eq.7 ($N_{low} < N_{cut}$). The integers n_{low} and N_{low} are then adjusted so as not to change the precision over the low energy eigenstates.

III. GAP AND PSEUDOGAP IN THE OPTICAL PHONON SPECTRUM

For different values of nonlinear coefficients A_3 and A_4 , we first examine the vibration spectrum of a one-dimensional (1D) lattice. The 2D lattice is treated at the end of the present section. When the non-quadratic part of the lattice energy is negligible, the eigen-spectrum of H is composed of the fundamental optical branch due to the harmonic phonon states (in Eq. 4, a single q verifies $n_q = 1$) and the branches due to the linear superpositions of these phonons (in Eq. 4, several q 's verify $n_q = 1$). The latest branches are stacked together into distinct bundles, each of them filling in a compact range of energy. In Fig. 3 and following ones, each eigenvalue of the finite size Hamiltonian is plotted as a single circle symbol. The distinct eigen-energies participate in different branches. The phonon branch is marked with the tag {1} while the branches that are due to the linear superposition of 2 phonon states are labelled by the tag {11}. For a macroscopic system, the bundle {11} covers a dense range of energy and forms a continuous band. The width of an optical phonon branch being physically a few percent of the elementary excitation energy, the dimensionless coupling C is fixed to $C = 0.05$ which gives, indeed a phonon branch width $\Delta_1 \approx 10\%$ of the phonon energy (see left inserts in Figs. 3-4). When nonlinearity is significant, the phonon branch shows no qualitative change (left inserts in Figs. 3(a) and 4(a)) in comparison with the fundamental optical branch in harmonic lattice. On the other hand, an isolated spectral branch is found in addition to the phonon branch and its combination tones (see Figs.3(a) and 4(a) and right-hand inserts). In Fig.5, varying artificially the coupling C from the trivial case $C = 0$, demonstrates that the additional branch coincides with the energy of the Bloch wave $B_{[\alpha,0,\dots,0]}$ with a single onsite excitation $\alpha = 2$. In Fig.3 and the next ones, the additional branch is marked with a single tag {2}. By analogy with biphonon theory¹, this branch is identified as the biphonon energy. Similar results are found for the triphonon states whose branch is labelled by the tag {3} in Fig.5. The reason for these isolated branches is that onsite Hamiltonian eigenvalues $\gamma_{\alpha>1}$ do not match the linear fit given by $(\gamma_1 - \gamma_0)\alpha + \gamma_0$. This is the consequence of h_l anharmonicity. The differences $\gamma_{\alpha>1} - [(\gamma_1 - \gamma_0)\alpha + \gamma_0]$ involve some gaps in the $C = 0$ spectrum which is composed of the Bloch wave energies. A moderate inter-site coupling hybridizes these states Eq.7 but the largest gaps remain (Fig. 5). The raising of degeneracy of $B_{[i,\alpha_i]}$ where only 2 α_i 's equal 1 and the rest are zero (number of these states is $S(S-1)/2$, their energy is $2\gamma(1) + (S-2)\gamma(0)$ at $C = 0$) yields a bundle of branches which correspond to the linear superposition of 2 single phonon states. In Fig.5, for higher energy, other bundles are labelled out by the tags {111} and {21}. At zero coupling, these branches coincide with the energies of states $B_{[1,1,1,0,\dots,0]}$ and $B_{[2,1,0,\dots,0]}$. For a macroscopic

lattice, the bundles $\{111\}$ and $\{21\}$ form some dense bands, as well as $\{11\}$. They are the unbound associations of 3 phonon states and of a biphonon with a single phonon, respectively. In Figs.3(a) and 4(a), for different parameters, the biphonon branch splits from the 2 phonons band. Measuring the energy of a biphonon state with reference to the unbound 2 phonons for same momentum q , a binding energy of biphonon is defined. A positive binding energy occurs when the onsite potential V is harder than a harmonic function (Fig.3(a)) whereas a softening yields a negative binding energy (Fig.4(a)). The biphonon energy gap is determined as the minimum of the absolute value of binding energy with respect to q . The biphonon gap reveals the strength of nonlinearity since when the biphonon gap overpasses the phonon branch width (as it does in Figs. 3(a) and 4(a)), it clearly indicates a significant contribution of non-quadratic terms. While in Figs.3(a) and 4(a), a biphonon gap opens, it is found that when nonlinearity is weak the biphonon binding energy vanishes at center of the lattice Brillouin zone (BZ) (Figs.3(b) and 4(b)). However, at the edge of BZ, the binding energy is comparable to the width of the phonon branch Δ_1 (inserts in Figs.3(b) and 4(b)). Consequently, a pseudogap is yielded when the non-quadratic energy has same magnitude as inter-site coupling. In this regime, the biphonon excitations exist only at the edge of BZ while they are dissociated into unbound phonons at center. With similar results, other calculations have been performed for different parameters. They showed that the biphonon pseudogap is a generic feature of lattices where nonlinearity is moderate. Similar pseudogaps have been noted in different quantum lattices^{19,20,21}. The pseudogap opens at the edge of BZ, even though the coupling sign is changed. So it is the q -range where nonlinear behavior is likely to be experimentally measured in materials where nonlinearity is weak.

In Fig.5, the low energy eigenvalues of H are plotted versus parameter C . The variations of the energy branches of the nonlinear excitations are labelled by tags defined previously. It can be noted that the widths of bound states branches increase with C much slower than unbound phonon bands. The branch of the α phonon bound states (biphonon for $\alpha = 2$ and triphonon for $\alpha = 3$) are found to merge with unbound phonon bands for a certain threshold C_α . At $C < C_\alpha$, the α^{th} branch and the unbound phonon bands are separated by a gap whereas around $C \approx C_\alpha$, only a pseudogap separates them partially. The C_α threshold depends on both coefficients A_3 and A_4 and it is different for each α phonon bound state branch because of anharmonicity. A unique set of nonlinear parameters A_3 and A_4 corresponds to the energy distribution of the biphonon and triphonon branches. So in principle, if a spectroscopy is able to measure the biphonon and the triphonon resonances, it is sufficient for inverting our numerical treatment and thus determining the nonlinear parameters. Moreover, the results in Fig.5 demonstrate that even though the non-quadratic terms in V are not large enough to open a biphonon gap, i.e., $C > C_2$ then a gap or at least a pseudogap opens for the α phonon bound states with $\alpha > 2$. Finally, the theoretical results in Fig.5(b) are qualitatively similar to the experimental findings in Ref.18 in which the Raman analysis of a molecular H_2 crystal shows a pressure-induced bound-unbound transition of the so called bivibron around 25 GPa. There is indeed a likeness between Fig.10 in Ref. 18 and the 2 phonon energy region in Fig. 5(b). In our model, the pressure variation of experiments¹⁸ can be simulated by a change of the coupling parameter C due to the fact that neighbouring molecules are moved closer together because of the external pressure. Actually, the increase of C induces a bound-unbound transition of the biphonon at $C = C_2$.

In Fig. 6, the diagonalization of a 2-dimensional (2D) lattice Hamiltonian is performed for $A_3 = 0$ and for different values of A_4 . The coupling amplitude is such as the phonon band width Δ_1 is a few percent of the elementary excitation branch. By estimating that $\Delta_1 \approx 2.d.|C|$, the value of the dimensionless coupling is fixed around $C = 0.025$. In the first overtone region, a gap opens when A_4 is large (top of Fig.6) whereas that gap closes at the center of the BZ when $A_4 = 0.025$ (bottom of Fig. 6). In the latter case, a pseudogap is found to open around $q = [11]$ and the width of that pseudogap has same order of magnitude as the phonon band width. These both quantities can be compared in the inserts of Fig.6 where the spectrum profile along $[11]$ is plotted. The pseudogap width is same as in Fig.3 for the 1D chain. Consequently, a pseudogap is expected for all lattice dimensions when both the inter-site coupling and the non-quadratic energy have a comparable magnitude.

IV. CORRELATION PROPERTIES OF THE PHONON BOUND STATES

In the present section, the study is focused on the space correlation in a 1D lattice. The space correlation function for displacements is defined as follows:

$$f(\Phi, n) = \sum_l \langle \Phi | X_l X_{l+n} | \Phi \rangle - \langle \Phi | X_l | \Phi \rangle \langle \Phi | X_{l+n} | \Phi \rangle \quad (10)$$

where Φ is an eigenstate and n is the dimensionless distance ($n > 0$). For an harmonic lattice, at weak inter-site coupling, it is easily verified that the single phonon correlation function is well approximated by $(\cos(qn))$. Then,

the correlation functions exhibit a space modulation with a constant amplitude. At $q = 0$, the function $f(\Phi, n)$ is a non-zero constant for all n .

Before discussing our results, it is convenient to compute analytically the function $f(\Phi, n)$ for the Bloch waves $B_{[\Pi_i \alpha_i]}$ (Eq. 7) with only one onsite excitation of order α . These states have the form:

$$B_{[\alpha, 0, \dots, 0]}(q) = \frac{1}{\sqrt{S}} \sum_j e^{-iq \cdot j} \phi_{\alpha, k+j} \cdot \prod_{l \neq k} \phi_{0, l+j}. \quad (11)$$

Let us introduce the notation, $\psi_\alpha(q)$ for these states. At the uncoupled limit ($C = 0$), the onsite excitation Bloch waves correspond to some eigenstates of H (see Fig.5 and text in Sec.III). The space correlation function of $\psi_\alpha(q)$ is given by:

$$f(\psi_\alpha(q), n) = 2D(\alpha, 0)^2 \cos(q n) - \frac{(D(\alpha, \alpha) - D(0, 0))^2}{S} \quad (12)$$

where $D(\alpha, 0)$ and $D(\alpha, \alpha)$ are defined in Eq.9. The constant term in the right hand side of Eq. 12 shrinks to zero when the lattice size S increases. In the numerical computations that are presented below, for finite lattices, that constant is removed in order to approach the behavior of the infinite lattices. Another point which is noteworthy is that, in general, the displacement operators are correlated for a given state $\psi_\alpha(q)$. Indeed the bracket $D(\alpha, 0)$ is usually not zero, except for even values of α when $A_3 = 0$, and the function $f(\psi_\alpha(q), n)$ shows a space modulation of amplitude $R_\alpha = 2D(\alpha, 0)^2$. The coefficients R_α are given in table Tab.I for parameters of Figs.3 and 4.

The function $f(\Phi, n)$ is plotted in Figs.7-9 for eigenstates Φ that are either the phonon, biphonon or the triphonon states. For each of these states, $f(\Phi, n)$ is computed for several values of q . The calculations at $C > 0$, demonstrate that the long range behavior of the correlation function for the α phonon bound states ($1 < \alpha < 4$) as well as for the phonon states ($\alpha = 1$) is similar to the variations of the function $f(\psi_\alpha(q), n)$, i.e., the modulations have same amplitudes for large distances. For a weak coupling, this property holds provided that the α^{th} discrete branch is separated from the rest of energy spectrum by some gaps. In Figs.7(a)-9(a), the correlation function of phonon states shows a modulation which extends over the whole lattice as in the pure harmonic lattice. For large n , the variations of $f(\Phi, n)$ are same as ones of $f(\psi_1(q), n)$, Eq. 12. Indeed, the amplitude of the modulations is given by the coefficient R_1 (see Tab. I). The correlated character of phonon states is thus related to the feature of the onsite excitation Bloch wave $\psi_1(q)$ and more precisely to the fact that the onsite displacement operator generates an overlap between the onsite groundstate $\phi_{0,i}$ and the first excited state $\phi_{1,i}$. The agreement between the long range behavior of phonon states and $\psi_1(q)$ holds in the harmonic lattice provided that C is not too large. This can be checked by comparing the formula $f(\Phi, n) = \cos(q n)$ for a single phonon state in the harmonic chain with the equation Eq.12, noting that for a quadratic form of V , we have $D(1, 0) = 1/\sqrt{2}$ and thus $R_1 = 1$.

The agreement between the coefficient R_α and the long range modulations of $f(\Phi, n)$ is not strictly proved for biphonon and triphonon (see Tab.I and Figs.7(b-c) and 8(b-c)) because the corresponding branches are too close from the unbound phonon bands. Nevertheless we estimate that the agreement roughly holds, whereas in Figs.9(b) it does not because the biphonon gap closes for small q . Provided the α^{th} discrete branch is isolated in the energy spectrum, there is no conceptual difference between α phonon bound states and single phonon states because they all come from the raising of the translational degeneracy of the onsite eigenstates $\phi_{\alpha,i}$. Actually, we conclude that the coefficient R_α is a good indicator of long range correlations for the α phonon bound states (including phonon states with $\alpha = 1$) on the condition that the hybridization with other phonon states is negligible. Therefore, when $R_\alpha = 0$, the α phonon bound states exhibit a finite correlation length provided the α^{th} discrete branch is isolated in the energy spectrum. In Fig.7(b), the space correlation function drops to zero for the large n and for all q in agreement with R_2 equals zero (see Tab.I).

As shown in Tab.I, $R_\alpha = 2D(\alpha, 0)^2$ decreases to zero with increasing α . Above $\alpha = 4$, R_α may be consider as physically negligible. By extension of our results about space correlations of the α phonon bound states with $\alpha < 4$, it is expected that the α phonon bound states with $\alpha \geq 4$ have a finite correlation length provided their energy branch remains isolated from the linear combination bands of the lower energy states, i.e., from the unbound phonon states as well as from the combinations of the lower order multi-phonon bound states (for instance, see {21} in Fig.5). For the specific case $A_3 = 0$ and $A_4 > 0$, the even values of α verify $R_\alpha = 0$, so the corresponding α phonon bound states have also a finite correlation length when their branch is isolated in the spectrum. For a closing biphonon gap, a pseudogap was found to persist at the edge of the lattice Brillouin zone (Sec.III). In Fig.9(b), it is shown that the biphonon states have a finite length scale in q -range where the pseudogap opens. Indeed, due to hybridization with the 2 phonon unbound states, the biphonons at $q \approx 0$ have a non-vanishing space correlation function which goes beyond the finite lattice size.

The phonon bound states with a finite correlation length exhibit a singular feature that is worth characterizing more precisely. For that purpose, denote by $\Phi_\alpha(q)$ the wave function of the α phonon bound state with momentum q and by $E_\alpha(q)$ the dimensionless energy of the α^{th} branch. One introduces the time dependent Wannier state $W_\alpha(t, n)$, which is constructed from a combination of the α phonon bound states:

$$|W_\alpha(t, k)\rangle = \frac{1}{\sqrt{S}} \sum_q e^{-i(q \times k + E_\alpha(q)\Omega t)} |\Phi_\alpha(q)\rangle. \quad (13)$$

The subscript k indicates the lattice site where is centered the Wannier transform. In Fig.10, the scalar product $|\langle \psi_\alpha(q) | \Phi_\alpha(q) \rangle|^2$ is plotted for $\alpha = \{1, 2, 3\}$. Fixing $A_3 = 0$ and $C = 0.05$, the parameter A_4 is increased from zero. The scalar product $|\langle \psi_\alpha(q) | \Phi_\alpha(q) \rangle|$ is proved to equal 1 when the gaps that surround the α^{th} branch are large, or equivalently when A_4 is large. Then, one can reasonably argue that the Bloch wave $\psi_\alpha(q)$ is a very good approximate of the α phonon bound state and the corresponding eigen-energy is approached by a perturbative theory:

$$\langle \psi_\alpha(q) | H | \psi_\alpha(q) \rangle = \gamma_\alpha + (S - 1)(\gamma_0 - CD(0, 0)^2) - C(R_\alpha \cos(q) + D(\alpha, \alpha)D(0, 0)). \quad (14)$$

When $A_3 = 0$, the correlation function $f(\psi_2, n)$ is zero for all n (since $R_2 = 0$, see Tab.I), so for the biphonon, we obtain $E_2(q) = \gamma_2 + (S - 1)\gamma_0$. Then the energy $E_2(q)$ does not depend on q , $E_2(q) = E_2$, and the Wannier state $|W_2(t, k)\rangle$ can thus be rewritten as follows:

$$|W_2(t, k)\rangle = e^{-i(E_2\Omega t)} \phi_{2,k} \prod_{l \neq k} \phi_{0,l}. \quad (15)$$

It is obvious that such a state is a localized and time periodic excitation. The classical counterparts of such state would be the breather solutions for the classical nonlinear discrete lattice, e.g. A. J. Sievers and S. Takeno¹². These classical breather solutions have two important features that are first their spatial localization and second their time periodicity with a frequency that is out of both the linear classical phonon branch and its resultant harmonic bands (for an exact proof see Ref.13). Our proposition about the classical counterparts could be justified by comparing the energies of a localized time periodic Wannier state and the semi-classical quantization of the classical breather orbits, in same lattice. In the simple case of zero inter-site coupling $C = 0$, such a comparison has been performed for the onsite double-well potential (see Fig.1(a) and text in Sec.II). The remarkable agreement obtained at $C = 0$, allows to expect that our proposition holds for weak values of C , at least. Extending our sketch to all α phonon bound states, the conditions for a breather-like Wannier state in a KG lattice are twofold: first, the branch of the α phonon bound states must be isolated by large surrounding gaps and second, $R_\alpha = 0$. Let us detail the breaking of these conditions. When the α^{th} branch is isolated but $R_\alpha > 0$, the $\psi_\alpha(q)$ are still some good approximates for the α phonon bound states (see in Fig.10 for the phonon and triphonon). Then the band width of the α^{th} branch does not vanish because of the self-tunneling of ψ_α , i.e., the intersite coupling hybridizes the Bloch wave $\psi_\alpha(q)$ with itself. The Wannier transform (Eq.13) of ψ_α is a combination of states non-coherent in time, since $E_\alpha(q)$ depends on q . It is no longer a time-periodic solution. After a certain time Δt_c , the Bloch waves ψ_α do no longer interfere. This Δt_c varies inversely to the band width of the α^{th} branch. On the other hand, when $R_\alpha = 0$ but the α^{th} branch is not isolated, the Bloch wave ψ_α is hybridized with unbound phonon states. Then the Wannier state in Eq.13 is no longer strongly localized as the breather-like Wannier state in Eq.15, but it shows some spacial extensions. In addition, $E_\alpha(q)$ depends on q (as shown in Fig.3(b), for the biphonon). Hence the Wannier transform is not coherent in time and $W_\alpha(t, k)$ is not time-periodic.

V. CONCLUSION

In the present paper, the pairing of phonon states in the nonlinear KG lattice has been considered with numerics. First, the biphonon spectral features have been studied and a pseudogap has been shown to characterize lattices where nonlinearity is comparable to phonon band width, whatever are the lattice dimension and the type of nonlinearity. Second, we have shown how properties of the KG biphonon depend on the nonlinearity. In the specific case of a strong ϕ^4 nonlinearity, the biphonon states feature a finite correlation length. The corresponding Wannier transforms are breather-like excitations that remain coherent for a duration which increases with the strength of the ϕ^4 nonlinearity. In contrast, when a ϕ^3 nonlinearity predominates, the biphonon exhibits a long range correlation and biphonon tunneling is no longer negligible, although it remains weaker than for single phonons. According to our results on the triphonon, one may expect that the tunneling of the high energy multi-phonon bound states vanishes for any type of nonlinearity, provided that their energy branches avoid the unbound phonon bands. Then some high energy breather-like excitations could occur. These states should correspond to the semiclassical quantization of the classical breather orbits.

I gratefully acknowledge financial support from Trinity College and an EC network grant on “Statistical Physics and Dynamics of Extended Systems” for the period spent at the University of Cambridge when these ideas were developed. Many thanks are addressed to Robert S. MacKay and Serge Aubry.

-
- ¹ V.M. Agranovich, *Spectroscopy and excitation dynamics of condensed molecular systems*, chp. 3, North-Holland publishing company (1983), pp. 83-138.
- ² J. C. Eilbeck, *Proceedings of the Third Conference Localization and Energy Transfer in Nonlinear Systems*, Eds. L. Vazquez, R. S. MacKay, M. P. Zorzano, World Scientific Singapore (2003), p.177.
- ³ F. Bogani, J. Phys. C: Solid State Phys. **11**, 1283 (1978).
- ⁴ V.M. Agranovich, Soviet Physics - Solid State **12**, 430 (1970).
- ⁵ F. Bogani, J. Phys. C: Solid State Phys. **11**, 1297 (1978).
- ⁶ S. Califano, V. Schettino and N. Neto, *Lattice dynamics of molecular crystals*, chp. 5, Springer-Verlag (1981),pp. 215-259
- ⁷ W.Z. Wang, J.T. Gammel, A.R. Bishop and M.I. Salkola, Phys. Rev. Lett. **76**, 3598 (1996).
- ⁸ R.S. Mackay, Physica A **288**, 174 (2000).
- ⁹ V. Hizhnyakov, D. Nevedrov and A. J. Sievers, Physica B **316-317**, 132 (2002).
- ¹⁰ J. Dorignac and S. Flach, Phys. Rev. B **65**, 214305 (2002); V. Fleurov, R. Schilling and S. Flach, Phys. Rev. E **58**, 339 (1998).
- ¹¹ V. Fleurov, Chaos **13**, 676 (2003).
- ¹² A. J. Sievers and S. Takeno, Phys. Rev. Lett. **61**, 970 (1988); S. Takeno, K. Kisoda and A. J. Sievers, Progress of Theoretical Physics Supplement **94**, 242 (1988).
- ¹³ R.S. MacKay and S. Aubry, Nonlinearity **7**, 1623 (1994).
- ¹⁴ L.D. Landau and E. M. Lifshits, *Quantum Mechanics (Non-Relativistic Theory)*, Pergamon Press, New York (1965).
- ¹⁵ when $E_d = 0.1$ eV and $b = 2$ Å, the parameters in Eq. (5) are $A_3 = -0.09496$, $A_4 = 0.00451$ and $\hbar\Omega = 0.02886$ eV.
- ¹⁶ William H. Press, *Numerical Recipes in Fortran*, Cambridge University Press (1992), pp. 462-475 ; <http://www.nr.com/> .
- ¹⁷ $\sqrt{2(w + \eta)} \rightarrow \Omega$ and $-\eta \rightarrow C.\Omega^2$, $v \rightarrow A_4.\Omega^3$ and $A_3 = 0$.
- ¹⁸ H. Mao and R.J. Hemley, Rev. Mod. Phys. **66**, 671 (1994).
- ¹⁹ N. Papanicolaou P. Spathis, J. Phys.: Cond. Matt. **1**, 5555 (1989).
- ²⁰ V. Pouthier and C. Falvo, Phys. Rev. E **69**, 041906 (2004).
- ²¹ J. Dorignac, J. C. Eilbeck, M. Salerno and A. C. Scott, Phys. Rev. Lett. **93**, 25504 (2004).

Table caption

Tab. I: Values of $R_\alpha = 2 \langle \phi_{\alpha,i} | X_i | \phi_{0,i} \rangle^2$ for different α and different nonlinear parameters, A_3 and A_4 used in Figs.3-9.

Figure captions

Fig. 1: Energy spectrum of a single He atom embedded into a double-well potential. The rank α of each eigenvalue $\gamma(\alpha)$ is given on the X-axis. (a) The semi-classical calculation (square symbols, dashed line) is compared to the Hamiltonian diagonalization (circle symbols, solid line) onto the truncated Einstein basis (see text below Eq.5) with a cutoff $N = 100$. The insert shows the double-well plot versus the displacement (in \AA). (b) The latter method is shown to converge to steady eigenvalues when the basis cutoff N increases ($N_\infty = 2000$).

Fig. 2: Eigen-spectrum of a $S = 4$ sites chain, with a ϕ^4 onsite potential. Model parameters are given in Ref. 17. Comparison between our numerics (circle symbols) and Ref. 7 (diamond symbols) (see Sec. II). The Y-axis unit is $\hbar\Omega$ and its zero is the groundstate energy. The X-axis bears the dimensionless first Brillouin zone.

Fig. 3: Eigen-spectrum of a $S = 33$ sites chain for parameters: (a) $C = 0.05$, $A_3 = 0$ and $A_4 = 0.2$ and (b) $C = 0.05$, $A_3 = 0$ and $A_4 = 0.02$. The inserts show magnifications of the fundamental branch (left) and the overtone region (right). The biphonon branch is marked by $\{\{2\}\}$ and the two-phonon band by $\{\{11\}\}$. The same tags label the inserts. The axis units are same as in Fig. 2.

Fig. 4: Same as Fig. 3 but for different nonlinear parameters: (a) $A_4 = 0.01$ and $A_3 = 0.13$ and (b) $A_4 = 0.01$ and $A_3 = 0.105$.

Fig. 5: Plot of the energy spectrum of a 1D chain, composed of $S = 19$ atoms for: (a) $A_4 = 0.2$, $A_3 = 0$. and (b) $A_4 = 0.01$, $A_3 = 0.13$, versus the dimensionless coupling C . Tags are explained in the text.

Fig. 6: (color online) On the left hand side, energy spectrum of a 2D square lattice in the region of the biphonon for $C = 0.025$, $A_3 = 0$ and $A_4 = 0.1$ (top) and for same parameters but $A_4 = 0.025$ (bottom). The lattice size is $S = 13 \times 13$. On the right hand side, profiles of the left-hand side spectra along the direction $[11]$. The inserts show the magnifications of the phonon branch (left) and the biphonon energy region (right).

Fig. 7: (color online) Plot of the correlation functions $f(\Phi, n)$ for 3 eigenstates of a $S = 23$ chain. Parameters are $A_4 = 0.2$, $A_3 = 0$, $C = 0.05$, versus the dimensionless distance n . The eigenstates are (a) phonon states, (b) the biphonon and (c) the triphonon with for each of them different wave vectors $q = 0$ (circles), $q = 4\pi/S$ (triangles), $q = 10\pi/S$ (diamonds), $q = 16\pi/S$ (squares) and $q = 22\pi/S$ (triangles). The inserts in (b) and (c) show a magnification of the zero y -axis.

Fig.8: (color online) Same as Fig. 7 but for $A_4 = 0.01$, $A_3 = 0.13$ and $C = 0.05$.

Fig. 9: (color online) Same as Fig.7 but for parameters $A_4 = 0.02$, $A_3 = 0$. and $C = 0.05$. The eigenstates are (a) the phonon states and (b) the biphonon.

Fig.10: Plot of the scalar product $|\langle \psi_\alpha(q) | \Phi_\alpha(q) \rangle|^2$ (see Sec. IV) for $C = 0.05$ and $A_3 = 0$ and for $q = 0$ (solid lines) and $q = \pi$ (dashed lines), versus the dimensionless parameter A_4 . The eigenstates are (a) the phonon states, (b) the biphonon states, and (c) the triphonon states.

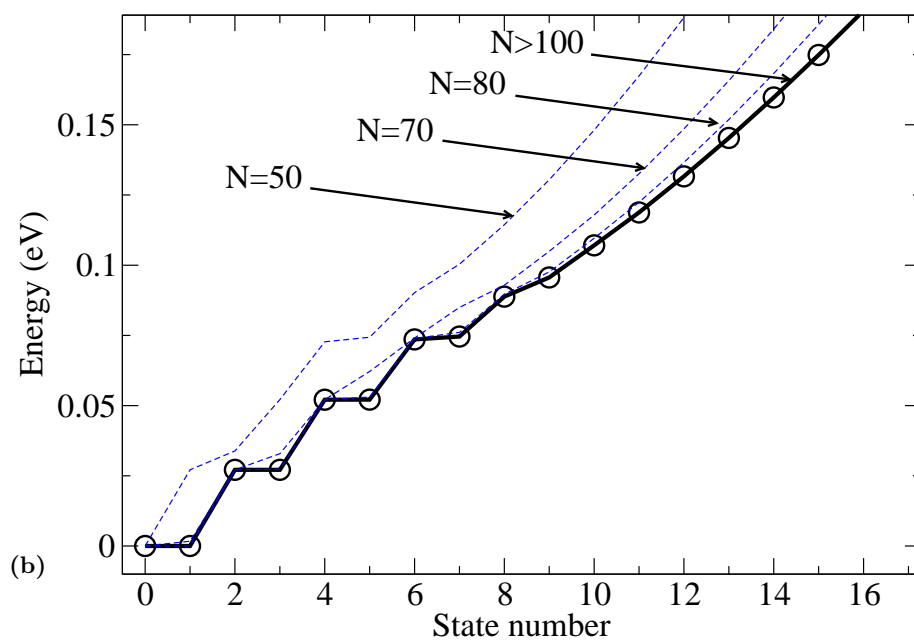
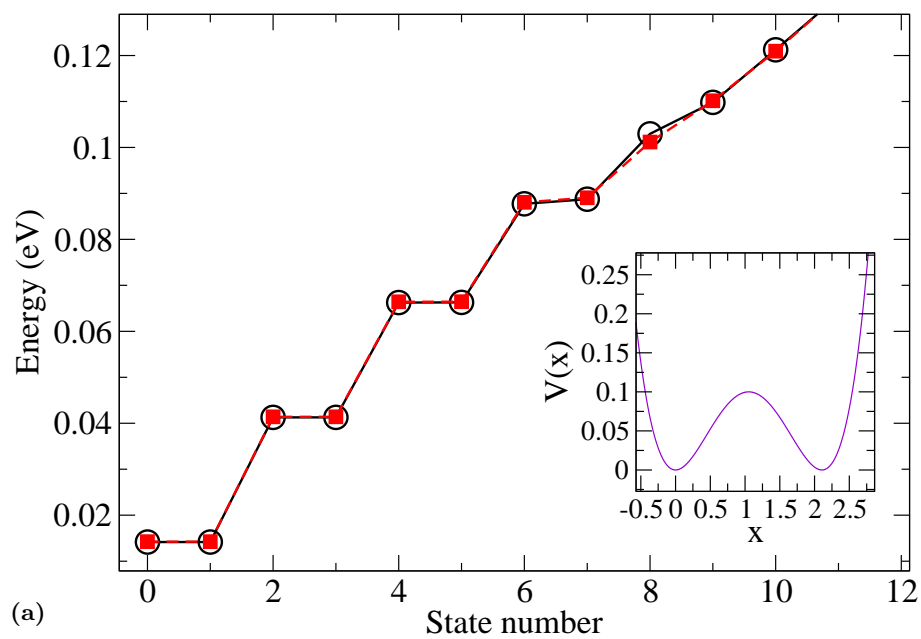


FIG. 1: (2004) L. Proville

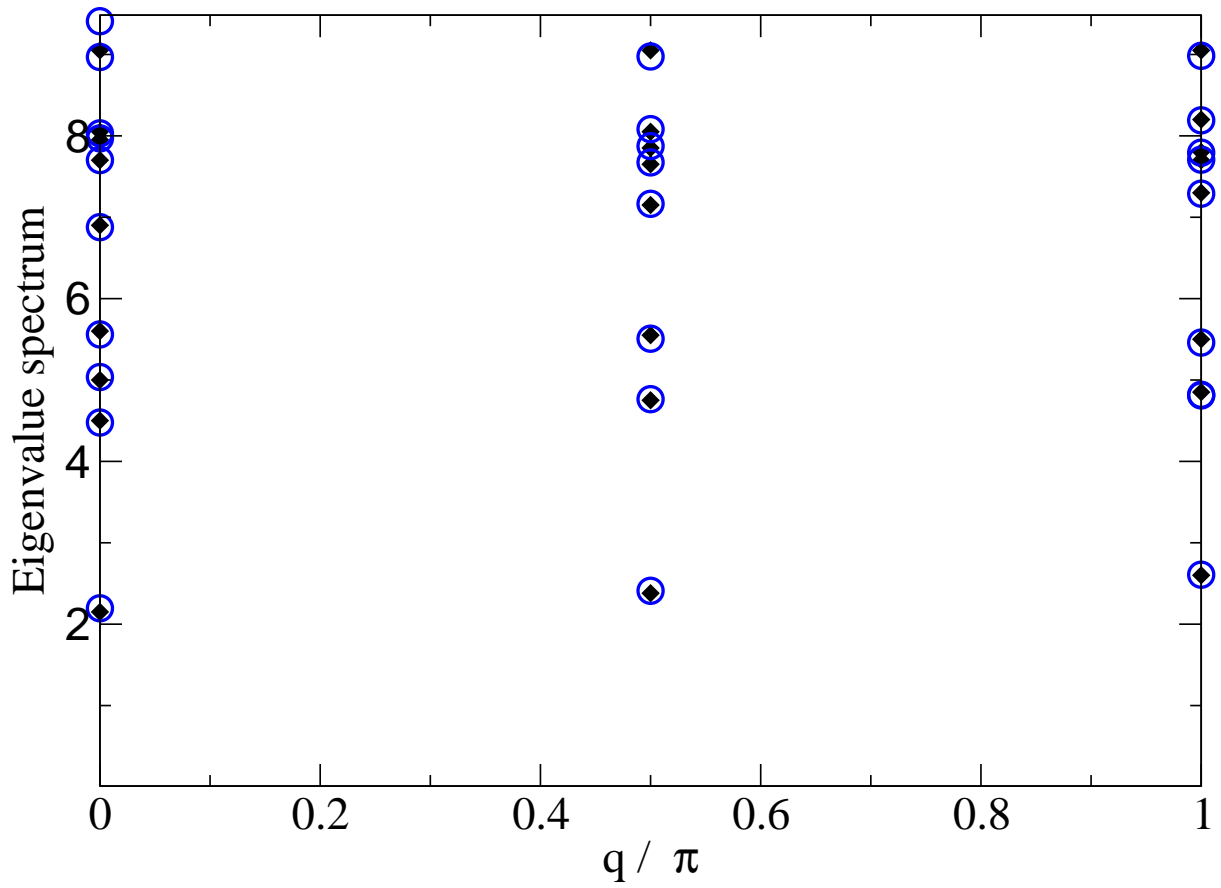


FIG. 2: (2004) L. Proville

$2 \langle \phi_{\alpha_i} X_i \phi_{0_i} \rangle^2$	$A_4 = 0.2 \ A_3 = 0$ Fig.3(a) & Fig.7	$A_4 = 0.01 \ A_3 = 0.13$ Fig.4(a) & Fig.8	$A_4 = 0.02 \ A_3 = 0$ Fig.3(b) & Fig.9	$A_4 = 0.01 \ A_3 = 0.105$ Fig.4(b)
$\alpha = 1$	0.74	1.06	0.95	1.03
$\alpha = 2$	0.	2.9710^{-2}	0.	1.1610^{-2}
$\alpha = 3$	7.3910^{-4}	2.3610^{-3}	7.910^{-5}	3.310^{-4}
$\alpha = 4$	0.	3.9110^{-4}	0.	1.0910^{-5}
$\alpha = 5$	8.4510^{-7}	5.4510^{-5}	1.4510^{-8}	4.3910^{-7}
$\alpha = 6$	0.	6.3810^{-6}	0.	1.9110^{-8}

TABLE I: (2004) L. Proville

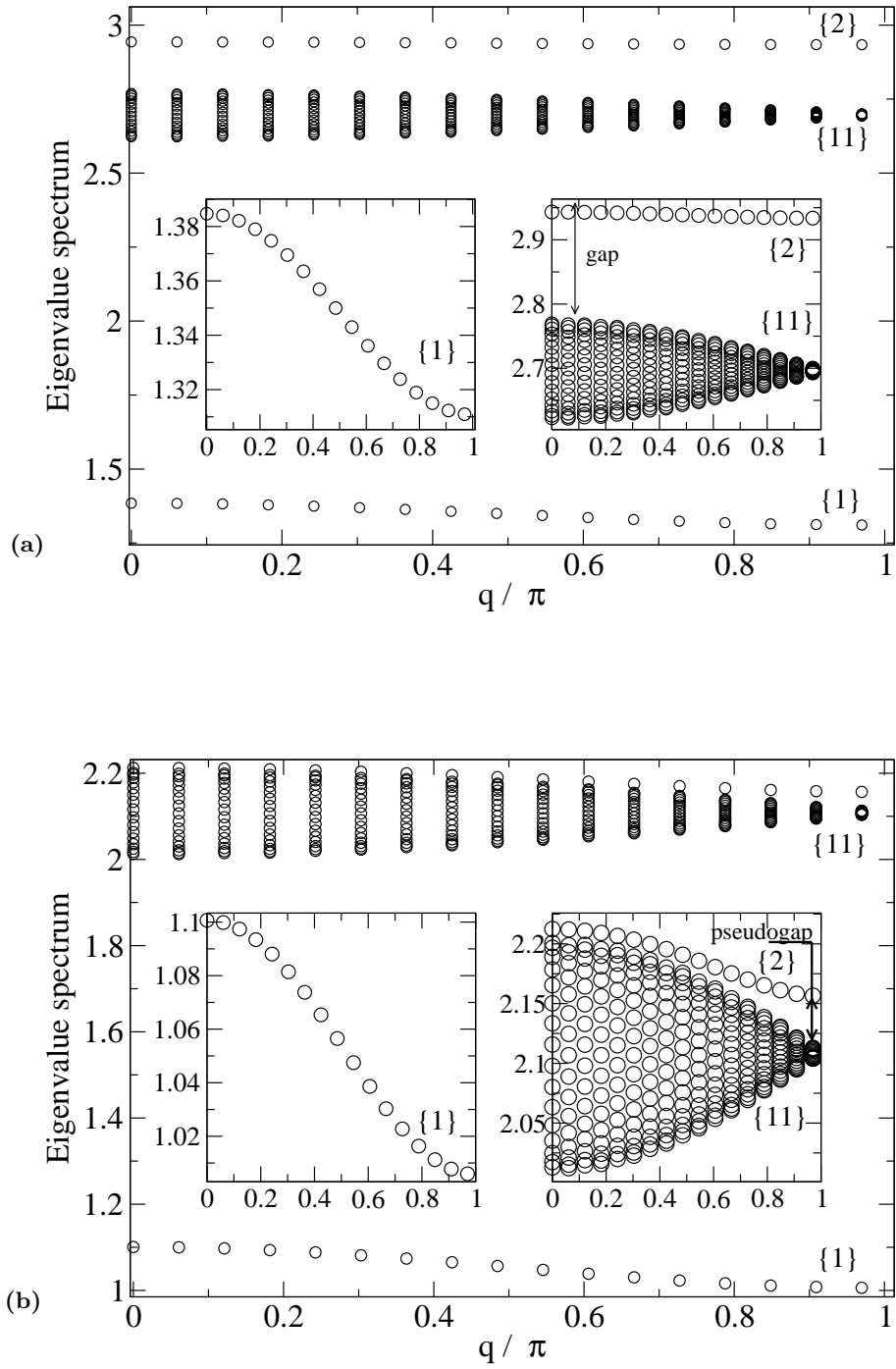


FIG. 3: (2004) L. Proville

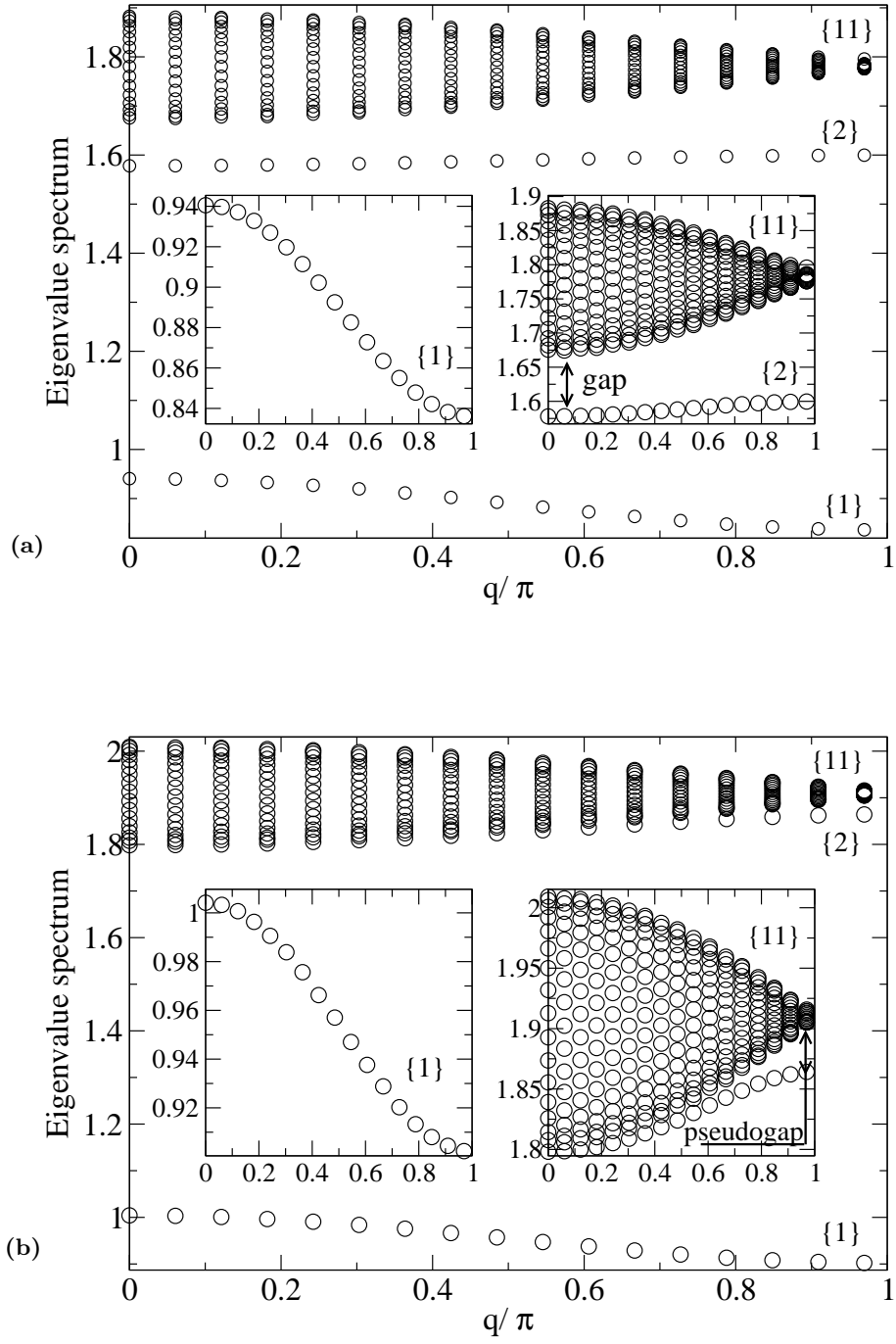


FIG. 4: (2004) L. Proville

FIG. 5: (2004) L. Proville: See additional figures

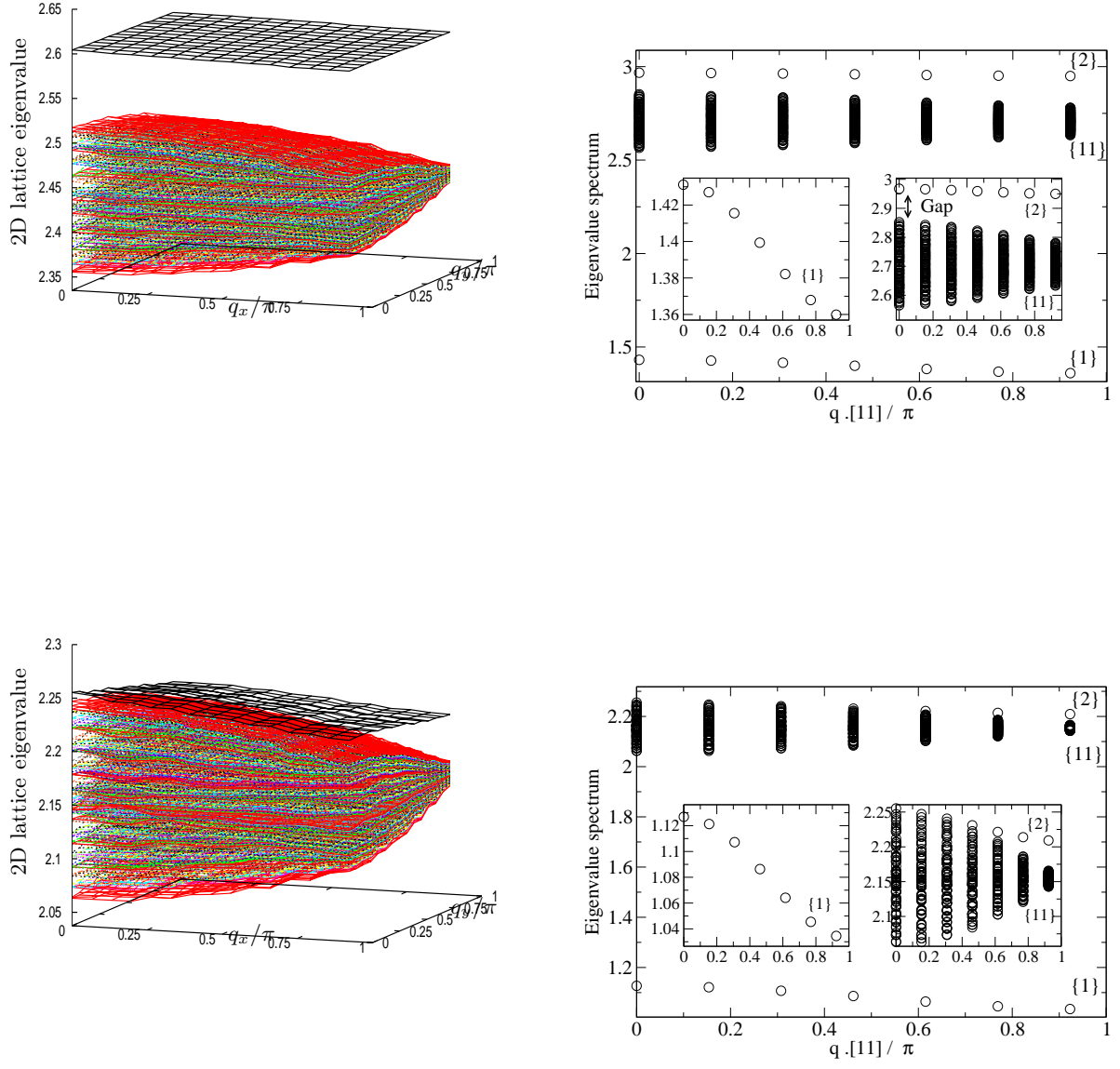


FIG. 6: (2004) L. Proville

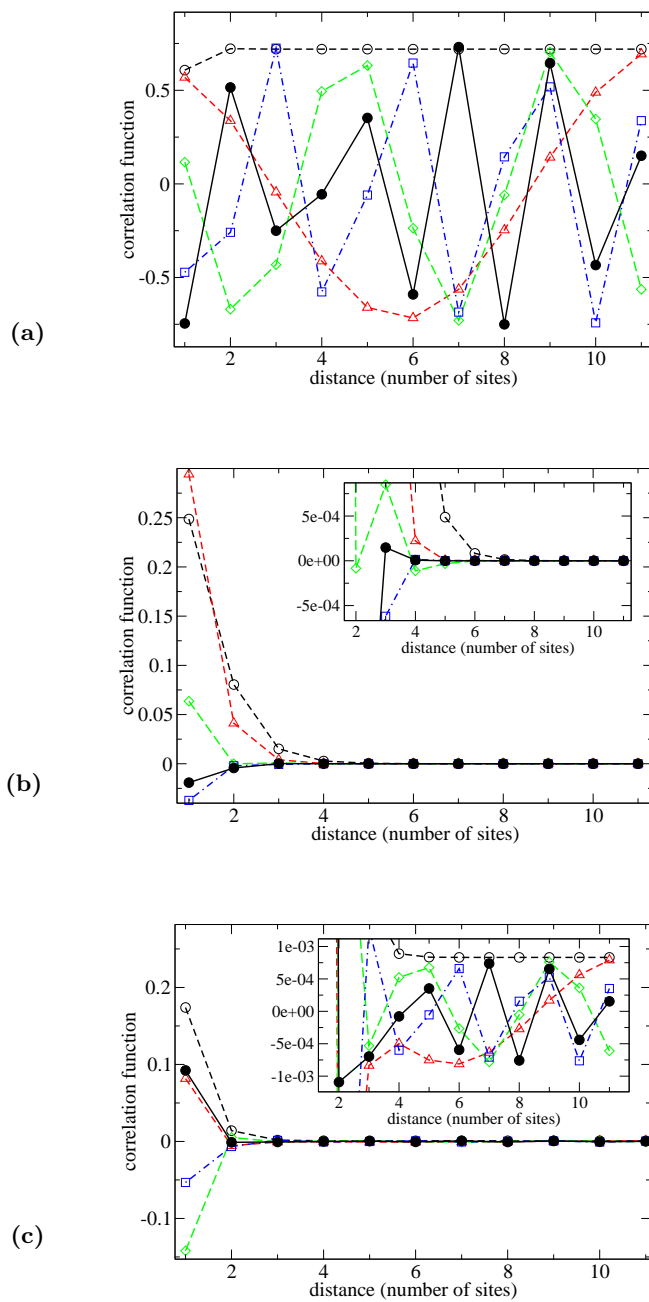


FIG. 7: (2004) L. Proville

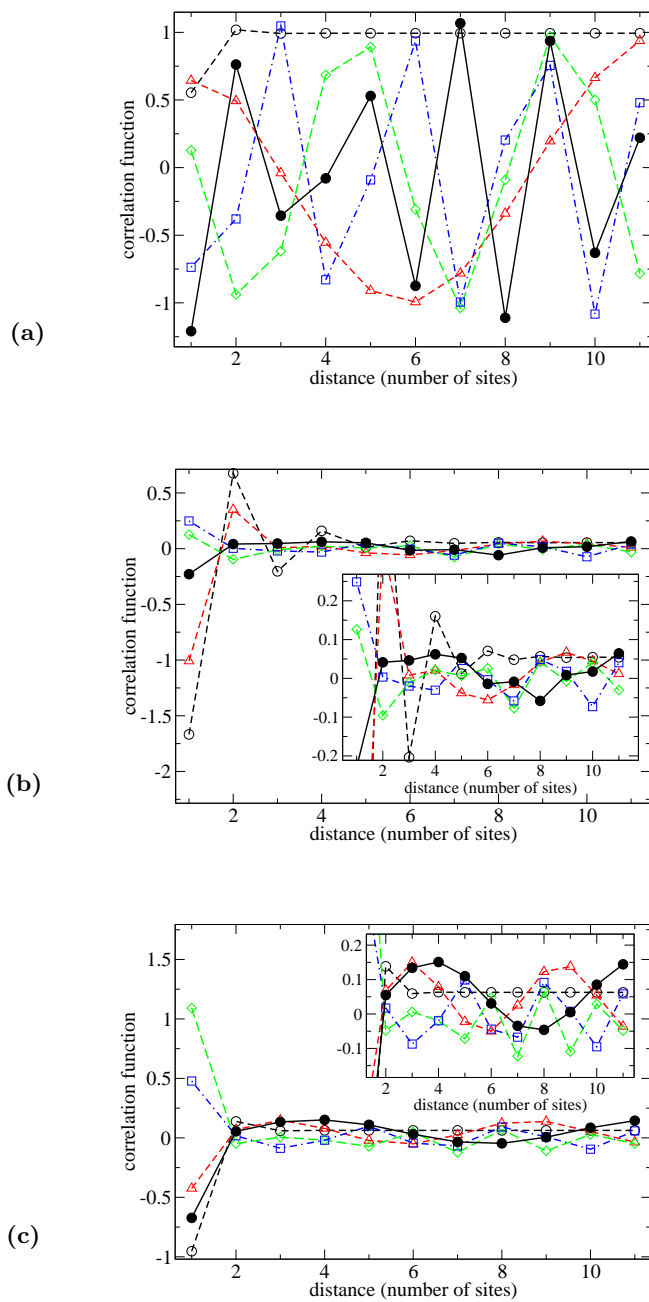
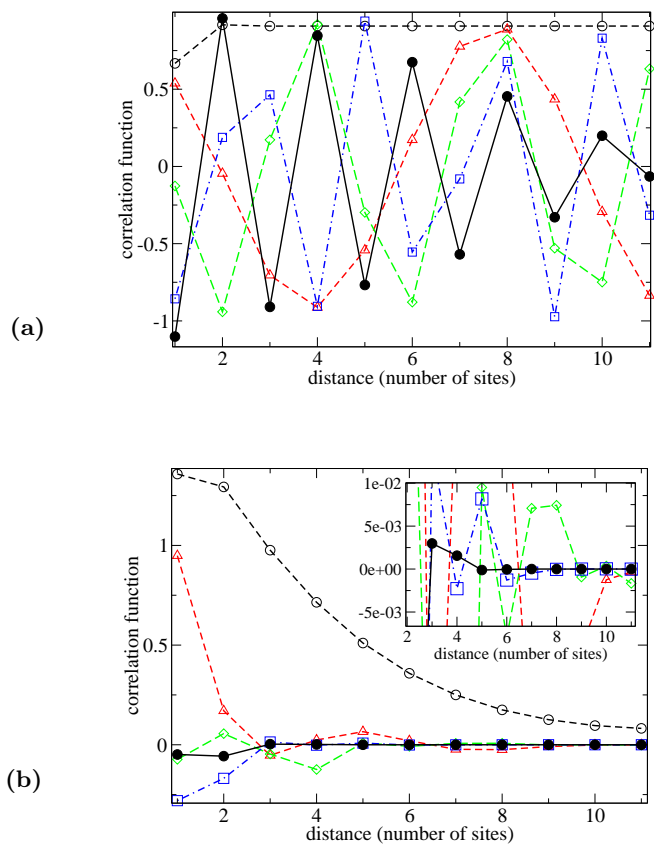


FIG. 8: (2004) L. Proville



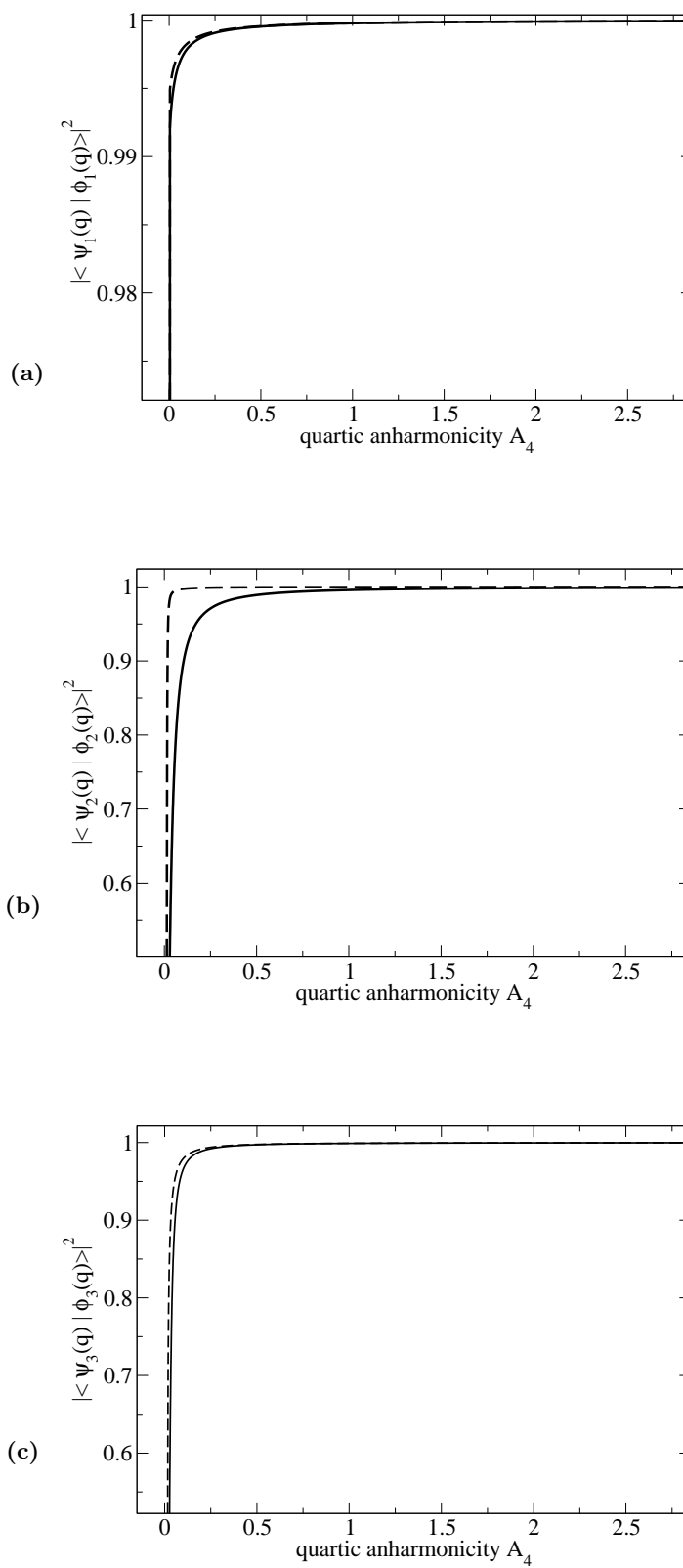


FIG. 10: (2004) L. Proville

This figure "fig7aPROVILLE.png" is available in "png" format from:

<http://arxiv.org/ps/cond-mat/0403516v6>

This figure "fig7bPROVILLE.png" is available in "png" format from:

<http://arxiv.org/ps/cond-mat/0403516v6>